IEEE Access
Multidisciplinary ⋮ Rapid Review ⋮ Open Access Journal

Received March 7, 2019, accepted April 3, 2019, date of publication April 11, 2019, date of current version April 25, 2019.

Digital Object Identifier 10.1109/ACCESS.2019.2910246

Temperature Dependent Analytical DC Model for Wide Bandgap MESFETs

SAIF-UR REHMAN, UMER F. AHMED, MUHAMMAD M. AHMED, (Senior Member, IEEE), AND MUHAMMAD N. KHAN
Department of Electrical Engineering, Capital University of Science and Technology, Islamabad 44000, Pakistan
Corresponding author: Muhammad M. Ahmed (mansoor@cust.edu.pk)

ABSTRACT In this paper, an analytical model has been developed to predict DC characteristics of wide bandgap metal semiconductor field effect transistors (MESFETs). The model evaluates potential distribution inside the channel of the device by dividing the Schottky barrier depletion layer into four distinct regions and predicts $I-V$ characteristics both at the room as well as at elevated temperatures. It also considers self-heating effects caused by the high-drain current and predicts negative output conductance, usually exhibited by wide bandgap MESFETs. The validity of the proposed technique is ensured by applying it on GaN and SiC MESFETs. It has been shown that the developed technique offers $\sim 50\%$ and $\sim 37\%$ improved accuracy in predicting the output characteristics of the device at $T = 300$ K and $T = 500$ K, respectively, relative to the best reported model. Thus, the proposed technique can be employed in the device modeling software involving high-power MESFETs.

INDEX TERMS MESFETs, analytical model, $I-V$ characteristics, self-heating effects.

I. INTRODUCTION

Wide bandgap semiconductors such as SiC/GaN are the preferred semiconductors used to fabricate power electronic devices. They have all the desired properties to fabricate a high quality metal semiconductor field effect transistor (MESFET). They have large energy bandgaps, which facilitate in the high voltage operation; high electron velocity, which enhances the switching frequency, and high thermal conductivity and melting point, which make the devices suitable for operation in high temperature and harsh environments [1], [2]. Dual metal gate design has suggested a further improvement in the device performance by suppressing short channel effects of the device [3], [4].

Due to high power applications and high switching speeds, SiC/GaN MESFETs suffer from self-heating effects because of the variation in the channel conditions [5], [6]. As the drain current (I_{DS}) increases, the temperature in the channel also increases and this in turn decreases mobility of carriers [7]. This leads to an overall reduction in the performance of a MESFET [8]. This degradation is further enhanced if the device is subjected to higher ambient temperature. However, in SiC/GaN MESFETs, these effects are relatively lower compared to other commercially used materials such as Si and GaAs [9]. Hence, SiC/GaN based devices can operate at a relative wider temperature range compared to Si/GaAs devices.

Self-heating effects should be taken into consideration while developing an analytical model; especially for wide bandgap semiconductor MESFETs, because they are primarily meant to operate at high bias and also at high switching speeds. Royet *et al.* in 2000 [5] developed an analytical model, incorporating self-heating effects, for long channel SiC MESFETs by dividing the gate depletion, underneath the Schottky barrier gate, into two regions: a region representing the depletion before the velocity saturation and the 2nd region of the depletion after the onset of velocity saturation. They proposed temperature dependent drift velocity using optical phonon coupling, which is difficult for a design engineer to handle.

In 2001, Bose *et al.* [10] developed an analytical model for GaN MESFETs DC characteristics. In their work, they used Poisson's equation to find the potential distribution across the depletion layer. Using this concept, they calculated the length after which the channel current saturates and eventually they developed an I_{DS} expression for the current flowing through the channel. However, their model did not consider variation in I_{DS} caused by self-heating effects which leads to limited applicability of the model.

The associate editor coordinating the review of this manuscript and approving it for publication was Anand Paul.

2169-3536 © 2019 IEEE. Translations and content mining are permitted for academic research only.
Personal use is also permitted, but republication/redistribution requires IEEE permission.
See http://www.ieee.org/publications_standards/publications/rights/index.html for more information.

Murray and Roenker [11] in 2002 developed a DC model for SiC MESFETs, wherein they divided the Schottky barrier depletion layer into two regions. They hypothesized that in each of the two regions, depletion height has its own distinct boundary conditions and these remain constant throughout the boundary. They calculated the potential distribution inside the channel and proposed an expression for the DC characteristics of the device. Murray *et al.* however, have not considered variation in the channel conditions associated with self-heating effects; thus, the model is bound to create discrepancy when the device is subjected to harsh operating conditions.

Zhu *et al.* [12] in 2006 extended the model proposed by Murray *et al.* by considering the extension of the depletion towards the drain side of the Schottky barrier gate. With the addition of the charges accumulated towards the drain side of the gate, they re-assessed potential distribution inside the channel and found that by ignoring the charge extension towards the un-gated drain side, it is not possible to model the characteristics of the device accurately; especially in the linear region of operation. Although, it is demonstrated that Zhu model is significantly better than Murray model in predicting the DC characteristics of a submicron SiC MESFET but, it is silent as far as self-heating or ambient temperature is concern.

Ahmed *et al.* [13] in 2017 re-evaluated the potential distribution inside the channel of submicron MESFETs by taking into account three distinct regions of the depletion layer underneath the Schottky barrier gate. They reported that the extension of the depletion layer towards the drain side, for submicron devices, is approximately one fourth of the gate length, L_g of the device. They demonstrated an improved accuracy of the modeled DC characteristics of submicron SiC MESFETs in comparison to Zhu model. Since, the model does not accommodate self-heating effects explicitly in its very definition, it would, therefore, bound to generate discrepancy for the devices having negative output conductance because of self-heating effects.

In this paper, an attempt has been made to develop a model to predict $I-V$ characteristics of wide bandgap MESFETs; especially those which exhibit self-heating effects in their output characteristics. This requires an accurate assessment of charge distribution inside the Schottky barrier depletion layer of the device. For this purpose, the depletion layer was distributed into four distinct regions, which facilitated an improved potential assessment inside the channel; leading to the development of an $I-V$ expression for the device output characteristics. Once an $I-V$ expression is established, it is then extended to incorporate self and ambient heating effects. The validity of the proposed model is demonstrated by using a variety of wide bandgap MESFETs.

II. MODEL DEVELOPMENT

An operating MESFET is shown in Fig. 1. In this figure, Region-I is the extension of the depletion towards the source side of the gate, whilst Region-II describes that part of the gate depletion where carriers are moving below the saturation velocity. The start of Region-III defines a location where channel carriers velocity gets saturated, and this region terminates at the end of the Schottky metal towards the drain side of the gate. And finally, Region-IV represents extension of the depletion towards the drain side caused by both the potentials i.e. V_D and V_G. The device output characteristics depend upon I_{DS} flowing through the channel under the influence of electric field E, and assuming that a is the epi-layer of the device as shown in Fig. 1, and $h(x)$ represents height of the depletion layer at any point x under the Schottky barrier gate; such that the available channel for the flow of I_{DS} is $[a-h(x)]$, then one can write [14]

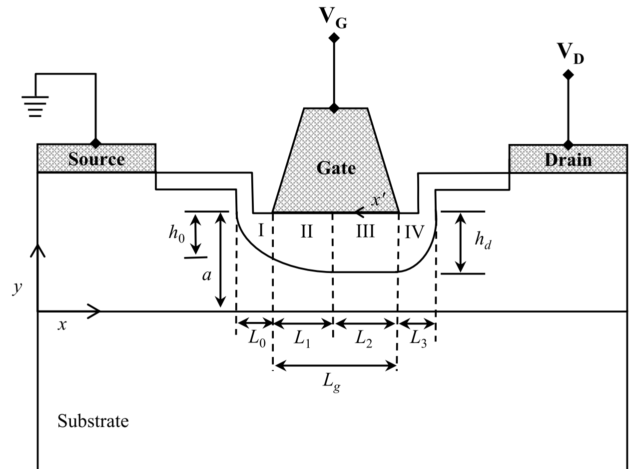

FIGURE 1. A cross-selectional view of a submicron MESFET.

$$I_{DS} = qWN\mu(E)E(x)\,[a-h(x)] \tag{1}$$

where q is the electronic charge, W is the width of the device, N is the channel doping density and $\mu(E)$ represents field dependent mobility of the channel carriers. An empirical relation, which defines $\mu(E)$ is given as [15], [16]

$$\mu(E) = \frac{\mu_0}{\left[1+\left(\dfrac{\mu_0 E}{v_s}\right)^{\beta}\right]^{1/\beta}} \tag{2}$$

where μ_0 represents low field mobility of carriers and its value shall be taken according to the chosen material of the MESFET either SiC or GaN, v_s is the carriers velocity after the onset of current saturation and β is a fitting variable.

In the linear region of operation, I_{DS} of the device increases linearly and its magnitude is dependent upon the bias potentials V_D and V_G. If we represent the linear region current by $I_{DS(\text{lin})}$, then it can be expressed as [11]

$$I_{DS(\text{lin})} = I_P\left[\frac{3(u_d^2-u_0^2)-2(u_d^3-u_0^3)}{1+Z(u_d^2-u_0^2)}\right] \tag{3}$$

In the above expression, u_d and u_0 are unit less quantities, which represent normalized depletion heights towards drain

and source side of the device, respectively; and are given by

$$u_d(V_G, V_D) = \frac{h_d}{a} = \sqrt{\frac{V_D + V_G + V_B}{V_P}}$$
$$u_0(V_G) = \frac{h_0}{a} = \sqrt{\frac{V_G + V_B}{V_P}} \quad (4)$$

where V_B is the built-in potential of the device; variables h_d and h_0 represent depletion layer heights towards drain and source side of the Schottky barrier gate, respectively. Device pinch-off voltage, V_P and other variables of above mentioned equations are given as

$$I_P = \frac{q^2N^2\mu_0 Wa^3}{6\epsilon_s L_g}, \quad V_P = \frac{qNa^2}{2\epsilon_s}, \quad Z = \frac{qNa^2\mu_0}{2\epsilon_s L_g v_s} \quad (5)$$

where ϵ_s is the relative permittivity of the semiconductor.

On the other hand, assuming that the current saturation in SiC/GaN MESFET is caused by the velocity saturation of the channel carriers, then the saturation current, $I_{DS(\text{sat})}$ can be expressed as [17]

$$I_{DS(\text{sat})} = qWN\gamma v_s a\,(1 - u_1) \quad (6)$$

where γ provides a smooth shift form the linear to the saturation region, and u_1 defines the depletion layer where carriers velocity gets saturated and is expressed as

$$u_1(V_G, V_D) = \frac{h_1}{a} = \sqrt{\frac{V(L_1) + V_G + V_B}{V_P}} \quad (7)$$

In Eq. (6) v_s shall be taken according to the chosen MESFET material either SiC or GaN to attain corresponding value of $I_{DS(\text{sat})}$. In Eq. (7), the variable $V(L_1)$ defines the potential across the length L_1 underneath the Schottky barrier gate as shown in Fig. 1 and is given by

$$V(L_1) = V_P\left(u_1^2 - u_0^2\right) \quad (8)$$

By using Eqs. (3) and (6), the channel length, L_1 can be evaluated in terms of device and bias parameters as given below [13]

$$L_1 = L_g Z\left[\frac{(u_1^2 - u_0^2) - (2/3)(u_1^3 - u_0^3)}{\gamma(1-u_1)} - (u_1^2 - u_0^2)\right] \quad (9)$$

To evaluate the two dimensional potential distribution of the Schottky barrier depletion as shown in Fig. 1, Poisson's equation, as given below, can be employed

$$\frac{\partial^2 V(x,y)}{\partial x^2} + \frac{\partial^2 V(x,y)}{\partial y^2} = -\frac{qN}{\varepsilon_s} \quad (10)$$

By changing co-ordinate system as shown in Fig. 1, i.e. $x' = x - L_g$, Eq. (10) can be rewritten as the sum of $W\left(x', y\right) = \xi\,(y) + V(x', y)$, where

$$\frac{d^2\xi}{dy^2} = \frac{qN}{\varepsilon_s} \quad (11)$$

and

$$\frac{\partial^2 W(x',y)}{\partial x^2} + \frac{\partial^2 W(x',y)}{\partial y^2} = 0 \quad (12)$$

such that

$$W\left(x', y\right) = V\left(x', y\right) + \frac{qN}{2\varepsilon_s}y^2 \quad (13)$$

Eq. (13) can be solved by employing the separation of variables technique and by using the device boundary conditions given as

$$\text{(i) } W(0, y) = -(V_G - V_B) + \frac{qNh_1 y}{\epsilon_s}$$
$$\text{(ii) } W(\acute{x}, 0) = -(V_G - V_B)$$
$$\text{(iii) } \frac{\partial W(0, h_1)}{\partial \acute{x}} = E_s$$
$$\text{(iv) } \frac{\partial W(\acute{x}, h_1)}{\partial y} = \frac{qNh_1}{\epsilon_s}$$

where, E_s is the saturation E. This gives

$$V\left(L_g, u_1\right) = V_P\left(u_1^2 - u_o^2\right) + \frac{2E_s a u_1}{\pi}\sinh\left[\frac{\pi\left(L_g - L_1\right)}{2au_1}\right] \quad (14)$$

First term of Eq. (14) represents the potential of Region-II; whereas, second term of Eq. (14) represents potential drop in Region-III. From Fig. 1, it is obvious that $L_2 = L_g - L_1$, therefore, the 2nd part of Eq. (14) is reduced to

$$V(L_2) = \frac{2E_s a u_1}{\pi}\sinh\left[\frac{\pi L_2}{2au_1}\right] \quad (15)$$

One can see from Fig. 1 that there is no Schottky barrier gate covering Region-IV; resultantly V_G will decay exponentially, causing the depletion layer to diminish quickly. Ahmed *et al.* [13] proposed that the length of Region-IV can be approximated as $L_3 \approx L_g/4$, resulting into

$$V(L_3) \approx \frac{2E_s a u_1}{\pi}\sinh\left[\frac{\pi L_3}{2au_1}\right] \approx \frac{2E_s a u_1}{\pi}\sinh\left[\frac{\pi L_g}{8au_1}\right] \quad (16)$$

In transverse direction, the total potential drop across the Schottky barrier gate will then be equal to the applied potential V_D, which can be written as

$$V(L_0) + V(L_1) + V(L_2) + V(L_3) = V_D \quad (17)$$

The combination of Eqs. (8), (15) and (16) forms the following equation

$$V_P\left(u_0^2\right) + V_P\left(u_1^2 - u_0^2\right) + \frac{2E_s a u_1}{\pi}\sinh\left[\frac{\pi\left(L_g - L_1\right)}{2au_1}\right] + \frac{2E_s a u_1}{\pi}\sinh\left[\frac{\pi L_g}{8au_1}\right] = V_D \quad (18)$$

Equation (18) gives potential distribution for all the four regions shown in Fig. 1. The first term $V_P\left(u_0^2\right)$ of Eq. (18), which is ignored in [13] has been included in this evaluation. Moreover, in [13] self-heating and temperature effects on the device $I - V$ characteristics have not been taken into consideration, which could lead to a discrepancy in the modeled

$I-V$ characteristics. In order to incorporate self and ambient heating effects, assume that R_S and R_D represent source and drain side resistances of the device, respectively; then drain to source voltage, V_{DS} can be written as

$$V_{DS} = V_D + I_{DS}(R_S + R_D) \tag{19}$$

such that

$$R_S = \frac{L_S}{Nq\mu aW} + R_C$$
$$R_D = \frac{(L_D - L_3)}{Nq\mu aW} + R_C \tag{20}$$

where R_C is the contact resistance and L_S and L_D provide separation between source-gate and drain-gate, respectively.

At ambient temperature, T, the thermal resistance, R_{TH} of a MESFET channel is defined as [18]

$$R_{TH} = \frac{1}{\pi\kappa} ln\left(\frac{8T}{\pi L_g}\right) \tag{21}$$

where κ represents thermal conductivity of the material involved. R_{TH} defined by Eq. (21) will change the response of the device based on power handled by it. Therefore, it is proposed that the channel resistance, R_{CH} can be written as

$$R_{CH} = R_{TH}\left(1 + \lambda\left[e^P - 1\right]\right) \tag{22}$$

where power, P is defined as $P = V_{DS}I_{DS}$ and λ will adjust the device channel geometry. In case there is no current flow, the device will not suffer from self-heating effect, as a result $R_{CH} = R_{TH}$. With increasing magnitude of I_{DS}, the channel will get heated; resulting into the reduction in carriers mobility due to an increase in R_{CH}, which translates into reduction in I_{DS}. This effect will vary from material to material which is adjusted by using optimized value of $\lambda_{\text{SiC}} = 0.13$ and $\lambda_{\text{GaN}} = 0.27$ defined in Eq. (22). Thus, the temperature dependent drain-to-source current, I_{DST} will be the current generated by the device by taking into account self and ambient heating, and it can be represented by the following expression

$$I_{DST} = I_{DS} - I_{DS}\left(1 - \frac{R_{TH}}{R_{CH}}\right) \tag{23}$$

In Eq. (23), R_{CH} is a dynamic function of the applied bias and its magnitude would be higher for higher values of I_{DS}, which would mean a pronounced negative conductance in the device output characteristics. Output conductance, G_{DT} can be obtained by differentiating Eq. (23), as given below

$$G_{DT} = \left.\frac{\partial I_{DST}}{\partial V_{DS}}\right|_{V_{GS}=\text{cont}} = \left.\frac{\partial\left[I_{DS} - I_{DS}\left(1 - R_{TH}/R_{CH}\right)\right]}{\partial V_{DS}}\right|_{V_{GS}=\text{cont}} \tag{24}$$

After making substitution for R_{CH} and differentiating, we have

$$\left.\frac{\partial I_{DST}}{\partial V_{DS}}\right|_{V_{GS}=\text{cont}} = \frac{\partial I_{DS}}{\partial V_{DS}}\left(\frac{1}{1 + \lambda\left[e^P - 1\right]}\right) + I_{DS}\frac{\partial}{\partial V_{DS}}\left(\frac{1}{1 + \lambda\left[e^P - 1\right]}\right) \tag{25}$$

If $\partial I_{DS}/\partial V_{DS} = G_D$, then Eq. (25) is reduced to

$$G_{DT} = \frac{G_D}{1 + \lambda\left[e^P - 1\right]} - I_{DS}\left(\frac{\lambda e^P\left(V_{DS}G_D + I_{DS}\right)}{\left(1 + \lambda\left[e^P - 1\right]\right)^2}\right) \tag{26}$$

Eq. (26) can also be written as

$$G_{DT} = \frac{G_D}{\left(1 + \lambda\left[e^P - 1\right]\right)^2}\left[\lambda e^P\left(1 - I_{DS}\right) - \lambda + 1 - \frac{I_{DS}^2}{G_D}\right] \tag{27}$$

When $V_{DS} < V_{DS(\text{sat})}$, under these conditions, $I_{DS} = I_{DS(\text{lin})}$ and $G_D = G_{DL}$; such that

$$G_{DL} = \left[\frac{3(1 - u_d) - 3Zu_d(u_d^2 - u_o^2) + 2Z(u_d^3 - u_o^3)}{\left(1 + Z(u_d^2 - u_o^2)\right)^2}\right] \times \frac{I_P}{V_P} \tag{28}$$

where use of Eqs. (3) and (4) is made to write Eq. (28). On the other hand, in the saturation region of operation, $V_{DS} \geq V_{DS(\text{sat})}$, under such circumstances, $I_{DS} = I_{DS(\text{sat})}$ and $G_D = G_{DS}$; such that

$$G_{DS} = \frac{-3\gamma I_P}{2Zu_1V_P} \times \left.\frac{\partial V(L_1)}{\partial V_{DS}}\right|_{V_{GS}=\text{cont}} = \frac{-3\gamma I_P}{2Zu_1V_P} \times \Gamma(V_{GS}, V_{DS}) \tag{29}$$

To achieve above mentioned expression, Eqs. (5), (6) and (7) are used. By differentiating Eq. (18) w.r.t V_{DS} at constant V_{GS}, and incorporating Eqs. (7) and (9), one can write function $\Gamma(V_{GS}, V_{DS})$ as

$$\Gamma(V_{GS}, V_{DS}) = \left[1 + \frac{E_s a}{\pi u_1 V_P}\left\{\sinh\left(\frac{\pi(L_g - L_1)}{2au_1}\right) - \frac{\pi}{2a}\cosh\left(\frac{\pi(L_g - L_1)}{2au_1}\right)\left\{\frac{L_g - L_1}{u_1} + L_g Z\left(\frac{(u_1^2 - u_o^2) - \frac{2}{3}(u_1^3 - u_o^3)}{\gamma(1 - u_1)^2} + 2u_1\frac{1 - \gamma}{\gamma}\right)\right\} + \sinh\left(\frac{\pi L_g}{8au_1}\right) - \frac{\pi L_g}{8au_1}\cosh\left(\frac{\pi L_g}{8au_1}\right)\right\}\right]^{-1} \tag{30}$$

Transconductance, G_{MT} can be expressed in a similar way as that of G_{DT} and the same is given below

$$G_{MT} = \left.\frac{\partial I_{DST}}{\partial V_{GS}}\right|_{V_{DS}=\text{cont}} = \left.\frac{\partial\left[I_{DS} - I_{DS}\left(1 - R_{TH}/R_{CH}\right)\right]}{\partial V_{GS}}\right|_{V_{DS}=\text{cont}} \tag{31}$$

By substituting R_{CH} and differentiating with respect to V_{GS}, we get

$$\left.\frac{\partial I_{DST}}{\partial V_{GS}}\right|_{V_{DS}=\text{cont}} = \frac{\partial I_{DS}}{\partial V_{GS}}\left(\frac{1}{1+\lambda\left[e^P-1\right]}\right) + I_{DS}\frac{\partial}{\partial V_{GS}}\left(\frac{1}{1+\lambda\left[e^P-1\right]}\right) \quad (32)$$

Considering $\partial I_{DS}/\partial V_{GS} = G_M$, Eq. (32) is transformed to

$$G_{MT} = \frac{G_M}{1+\lambda\left[e^P-1\right]} - I_{DS}\left(\frac{\lambda e^P V_{DS} G_M}{\left(1+\lambda\left[e^P-1\right]\right)^2}\right) \quad (33)$$

Above expression can also be written as

$$G_{MT} = \frac{G_M}{\left(1+\lambda\left[e^P-1\right]\right)^2}\left[\lambda e^P(1-P)-\lambda+1\right] \quad (34)$$

When $V_{DS} < V_{DS(\text{sat})}$, under these conditions, $I_{DS} = I_{DS(\text{lin})}$ and $G_M = G_{ML}$; such that

$$G_{ML} = \left[\frac{(u_o-u_d)+Zu_ou_d(u_d+u_o)-Z(u_d^3-u_o^3)}{\left(1+Z(u_d^2-u_o^2)\right)^2}\right] \times \frac{3I_P}{V_P} \quad (35)$$

On the other hand, when $V_{DS} \geq V_{DS(\text{sat})}$, this resulted into $I_{DS} = I_{DS(\text{sat})}$ and $G_M = G_{MS}$; such that

$$G_{MS} = \frac{3\gamma I_P}{2Zu_1V_P}\left[\frac{L_gZE_s}{V_P}\left\{\frac{(1-u_0)-\gamma(1-u_1)}{\gamma(1-u_1)}\right\} \times \cosh\left(\frac{\pi(L_g-L_1)}{2au_1}\right)\right]\Gamma(V_{GS},V_{DS})$$

In writing the above expression, use of Eqs. (6), (18) and (30) is made.

III. MODELED CHARACTERISTICS

To ensure the validity of the developed technique, MESFETs of varying L_g and W were selected and their DC characteristics were modeled and compared with the experimental data. Table 1 represents physical parameters of the selected devices. The chosen GaN MESFET was fabricated by [19] on a 200 nm thick n-GaN active layer grown using metal organic chemical vapor deposition upon a sapphire substrate. Prior to active layer formation, a 3.6 μm thick undoped buffer layer along with a 25 nm thick nucleation layer was also deposited to improve the quality of the active layer. Devices were fabricated using standard lithography and lift-off processes and the finished device physical dimensions are given in Table 1. On the other hand, the detail of chosen SiC MESFET are given in [7], wherein recessed type devices were realized using heavily doped contact layer upon a moderately doped channel layer. The layer structure including the buffer layers were grown by chemical vapor deposition technique upon a semi-insulating SiC substrate. Devices were fabricated using lift-off process and the physical dimensions of a finished SiC MESSFET along with its electrical parameters are elaborated in Table 1. Room and high temperature measurements of the finished but unpacked devices were carried out using on-wafer direct measurements.

TABLE 1. Physical parameters of GaN/SiC MESFETs.

Parameters	GaN [19]	4H-SiC [7]
gate Length, L_g (μm)	0.3	1.0
Gate Width, W (μm)	100	500
Epi-layer thickness, a (μm)	0.2	0.3
Doping Density, N ($\times 10^{17}$ cm^{-3})	2.7	1.1
Gate-Source Separation, L_S (μm)	1.0	0.5
Gate-Drain Separation, L_D (μm)	2.3	2.0
Thermal Conductivity, κ (W/m-K)	160	490
Electron Mobility, μ (cm^2/Vs)	1000	700
Built-in Potential, V_B (V)	1.3	1.1
Band-Gap, E_g (eV)	3.49	3.26
Saturation Velocity, v_s ($\times 10^7$cms^{-1})	2.5	2.2

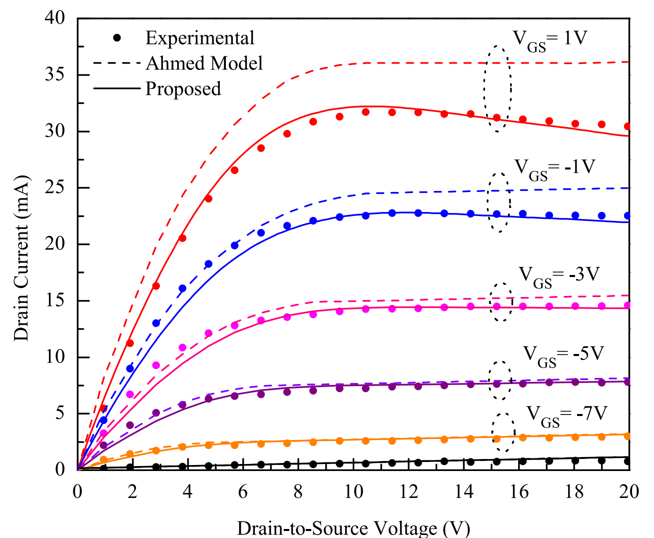

FIGURE 2. Modeled and experimental [19] DC characteristics at $T = 300$ K of a 0.3 μm GaN MESFET for $V_{GS} = 1$ V to -9 V with a step of 2 V.

By using Eq. (23), the device output characteristics can be plotted, which incorporate both the self-heating as well as the ambient temperature effects on the device performance. The expression does not include the effect of temperature which could be caused by the devices mutual conductance for an integrated circuit. Figure 2 shows measured [19] and modeled output characteristics of a GaN MESFET. Dotted lines, as shown in the figure, represent a significant deviation

TABLE 2. Bias dependent RMS error values between the modeled and the experimental output characteristics of a 0.3 μm GaN MESFET. Bold faces show lowest observed values.

Model	V_{GS}						Avg.
	1 V	−1 V	−3 V	−5 V	−7 V	−9 V	
Ahmed	0.8620	0.3736	0.2116	0.1583	0.1272	0.2236	0.3261
Proposed	**0.1132**	**0.1591**	**0.1829**	**0.1337**	**0.1051**	**0.2203**	**0.1524**

from the experimental data, especially in the saturation region of operation. Moreover, this deviation is more pronounced at higher drain current. Since at higher drain current, self-heating effects are also higher and the model presented in [13] does not consider the self-heating effects in its very development; resultantly there is deviation from the experimental data. It is pertinent to mention here that the performance of the model presented in [13] improves when output conductance of the device, in the saturation region of operation, is either zero or positive. As the model is not designed for negative conductance of the device; thus, it is bound to generate relatively higher errors if the device exhibits negative conductance after the onset of current saturation.

In Fig. 2, solid lines show characteristics drawn with the proposed modified model. A significant improvement can be seen when compared with [13]. The observed improvement is both in the linear as well as in the saturation region of operation, which is primarily due to the inclusion of self-heating term in the model expression. Table 2 shows bias dependent root mean square (RMS) errors for the proposed model relative to the experimental data. For comparison purposes, errors obtained from the model presented in [13] are also listed. Examining the data of the table, it is obvious that the proposed model has outperformed [13] in all reported values of V_{GS}. And on the average, the proposed model exhibited $\sim$ 53% improvement in predicting the DC characteristics of a GaN MESFET.

Figure 3 shows measured [7] and modeled output characteristics of a 1 μm SiC MESFET at $T = 300$ K. Once again, it is obvious from the figure that the proposed model performance is significantly better than the model presented in [13]. It is pertinent to mention here that at $V_{GS} = 0$ V, there is maximum current flowing from the channel; resulting into larger heat dissipation thus, higher negative conductance in the saturation region of operation is seen in Fig. 3. In conformity to Fig. 2, there is more discrepancy in this case between the model presented in [13] and the experimental data. This effect is subsequently improved for the cases where less magnitude of I_{DS} is flowing from the channel. Contrary to this, the proposed model provides, in general, improved performance irrespective of the gate bias thus, indicating its ability to predict $I-V$ characteristics of wide bandgap MESFETs designed for power and harsh environment applications, independent of their fabrication material. Furthermore, it is also noted that the model is capable to predict $I-V$ characteristics for the long channel ($L_g = 1$ μm) as well as for the short channel ($L_g = 0.3$ μm) devices, fabricated using wide bandgap material, exhibiting its wider applicability, provided the material properties remain intact. On the other hand, this model may not be fully valid for MESFETs having different physical structure then the one chosen in this research. Because, in that case Poisson's equation solution could be different; leading to a changed potential distribution inside the channel and hence a changed response.

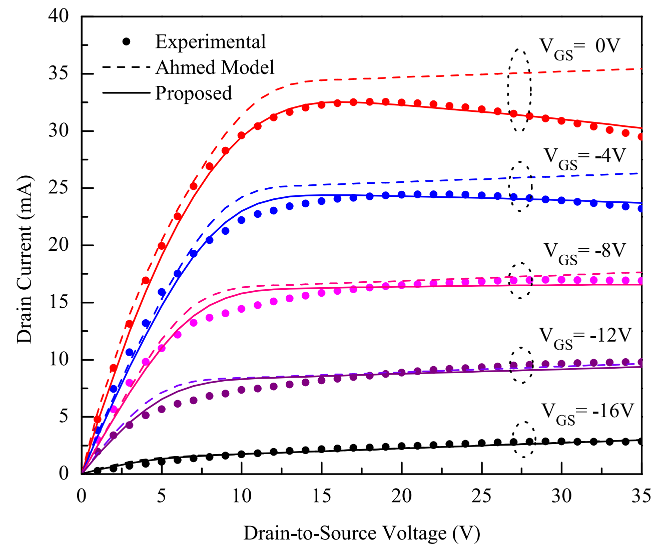

FIGURE 3. Modeled and experimental [7] DC characteristics at $T = 300$ K of a 1 μm SiC MESFET for $V_{GS} = 0$ V to −16 V with a step of 4 V.

Table 3 shows V_{GS} dependent RMS error values, at $T = 300$ K, for the proposed and Ahmed model for a SiC MESFET whose characteristics are shown in Fig. 3. It is obvious from the data of the table that the proposed model performance is relatively better than Ahmed model for values of V_{GS} considered for error evaluation. On average, the proposed model achieved $\sim$ 54% improved performance relative to Ahmed model.

Figure 4 shows measured and modeled output characteristics, once again, for the device of Fig. 3 but, at $T = 500$ K. It is an established fact that at elevated temperature the channel offers increased scattering, which reduces the mobility and also the saturation velocity of the carriers; resulting into reduced I_{DS}. This fact is evident from the $I-V$ characteristics of Fig. 4. Examining the plots of Fig. 3 and 4 simultaneously,

TABLE 3. Bias and temperature dependent RMS error values in modeled output characteristics of a 1 μm SiC MESFET. Bold faces show lowest observed values.

Temp.	Model	V_{GS} 0 V	-4 V	-8 V	-12 V	-16 V	Avg.
$T = 300$ K	**Ahmed**	0.5576	0.3612	0.2379	0.2525	0.1319	0.3082
	Proposed	**0.0798**	**0.1229**	**0.1635**	**0.2122**	**0.1163**	**0.1390**
$T = 500$ K	**Ahmed**	0.2652	0.1865	0.0869	0.0889	**0.1435**	0.1542
	Proposed	**0.1035**	**0.1004**	**0.0605**	**0.0771**	0.1443	**0.0972**

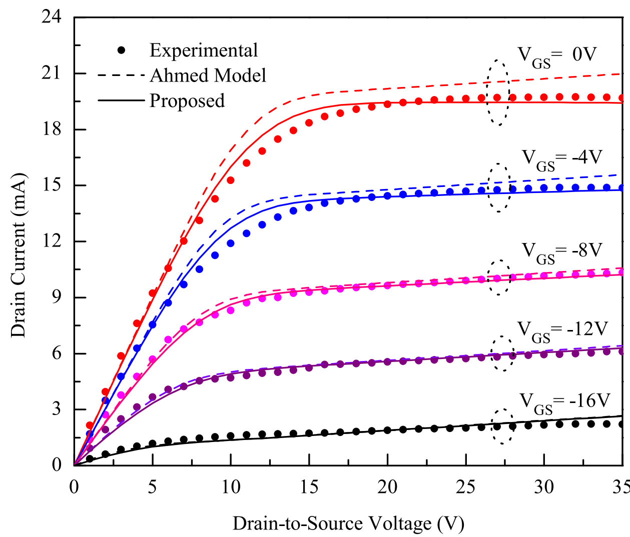

FIGURE 4. Modeled and experimental [7] DC characteristics at $T = 500$ K of a 1 μm SiC MESFET for $V_{GS} = 0$ V to -16 V with a step of 4 V.

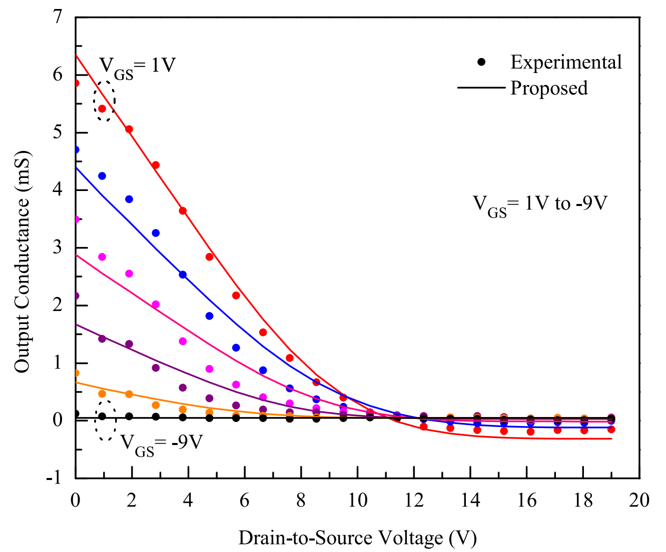

FIGURE 5. Modeled and experimental [19] output conductance of 0.3 μm GaN MESFET at $T = 300$ K.

it is evident that by increasing the temperature from $T = 300$ K to $T = 500$ K, the magnitude of I_{DS} reduces to almost 50%. Since the device current is reduced, the negative conductance in the saturation region of operation, as discussed before, also reduces. It has been observed earlier that at relatively lower current, there is an improvement in the performance of Ahmed model and the same is reflected by the characteristics shown in Fig. 4. An improved performance by Ahmed model at $T = 500$ K relative to $T = 300$ K cannot be associated with the model expression, because the model expression does not take into account the ambient temperature as a variable. Rather, this improvement is due to the lowering of I_{DS}, which also lowered the negative output conductance of the device, especially, at $V_{GS} = 0$ V. Thus, reducing the gap between the modeled and observed output characteristics. This fact is also evident from the data of Table 3, where the gap between observed RMS errors for the proposed and the model presented in [13] evaluated at $T = 500$ K is relatively lower and the average RMS error for the proposed model shows $\sim 37\%$ improvement, which is lower than the earlier two reported values.

Eq. (27) is valid for the entire range of V_{DS} bias and a plot of G_{DT} as a function of V_{DS} with V_{GS} as a variable is shown in Fig. 5. It can be seen from the figure that the modeled characteristics show a reasonable compliance to the experimental data. According to our conservative estimate, there is no reported model for SiC/GaN MESFETs, which can predict the negative G_D of the device, especially, in the saturation region of operation. The proposed model has the ability to give both negative as well as positive values of G_D with reasonable accuracy.

Table 4 shows RMS error values of the two competing models for a 0.3 μm GaN MESFET, whose $I - V$ characteristics are shown in Fig. 2. It is obvious from the outcome presented in Table 4 that at medium gate bias ($V_{GS} = -3$ to -5 V), the performance of the model presented in [13] is better than the proposed model, however, the proposed model, in general, offers improved performance, as evident from the data of Table 4, and on the average, its performance is $\sim 25\%$ better than Ahmed model.

Figures 6 and 7 show experimental and modeled G_D of a 1 μm SiC MESFET at $T = 300$ K and $T = 500$ K, respectively. Both the figures are once again validating the proposed Eq. (27) representing drain conductance (G_{DT}) of wide bandgap MESFETs, both at room as well as at elevated temperature of operation. Table 5 represents RMS error

TABLE 4. Bias dependent RMS error values between the modeled and the experimental output conductance of a 0.3 μm gate length GaN MESFET. Bold faces represent lowest error values.

Model	V_{GS}						Avg.
	1 V	−1 V	−3 V	−5 V	−7 V	−9 V	
Ahmed	0.6201	0.2647	**0.1987**	**0.2007**	0.1676	0.1309	0.2638
Proposed	**0.1363**	**0.2242**	0.2825	0.2511	**0.1504**	**0.1297**	**0.1957**

TABLE 5. Bias and temperature dependent RMS error values between the modeled and the experimental output conductance of a 1 μm gate length SiC MESFET. Bold faces represent lowest error values.

Temp.	Model	V_{GS}					Avg.
		0 V	−4 V	−8 V	−12 V	−16 V	
$T = 300$ K	**Ahmed**	0.2530	0.2259	0.2380	0.1917	0.1882	0.2194
	Proposed	**0.1107**	**0.2043**	**0.2248**	**0.1834**	**0.1394**	**0.1725**
$T = 500$ K	**Ahmed**	0.1824	0.1569	0.1063	**0.0926**	**0.1111**	0.1299
	Proposed	**0.1362**	**0.1166**	**0.1035**	0.1109	0.1231	**0.1180**

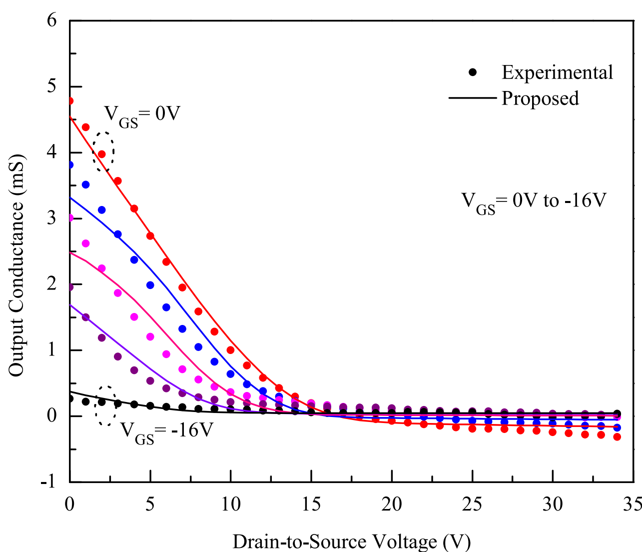

FIGURE 6. Modeled and experimental [7] output conductance of 1 μm SiC MESFET at $T = 300$ K.

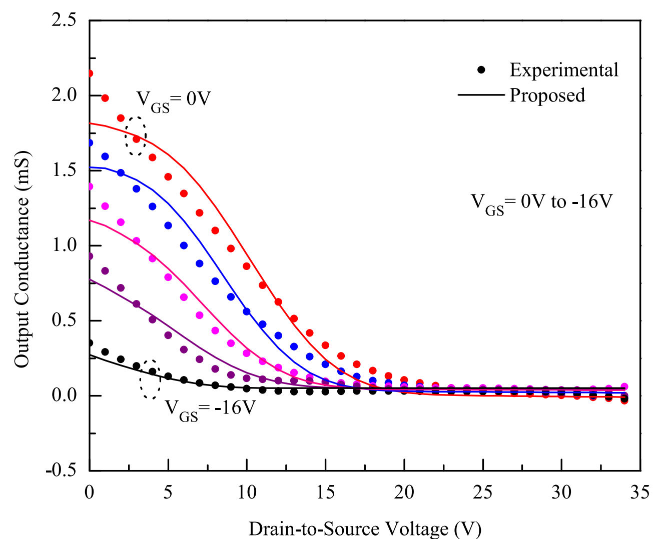

FIGURE 7. Modeled and experimental [7] output conductance of a 1 μm gate length SiC MESFET at $T = 500$ K.

values for the two temperatures under discussion. Average observed improvement relative to Ahmed model is $\sim 21\%$ and $\sim 9\%$ at $T = 300$ K and $T = 500$ K, respectively. This demonstrates that the improvement offered by the proposed model is device and ambient dependent. However, in general, the proposed model is relatively better than the best reported analytical model for wide bandgap MESFETs. It is pertinent to mention here that though Ahmed model does not incorporate temperature dependent variable to adjust negative conductance in the saturation region of operation yet it adjusts the value of G_{DT} at $T = 500$ K by adjusting the variable γ, which appears in its definition.

A plot of Eq. (34) for $L_g = 1$ μm SiC MESFET is shown in Fig. 8, at $T = 300$ K (solid symbols) and $T = 500$ K (open symbols). In the figure, $V_{DS} = 5$ V curves show response of the device in the linear region of operation; whereas, $V_{DS} = 35$ V curves indicate the device G_{MT} for the saturation region of operation for the two temperatures under consideration. Examination of the figure clearly reveals that at $T = 500$ K, the G_M of the device is deteriorated, which could primarily be associated with the reduction in I_{DST} at elevated temperature.

An interesting feature, which can be noted from the plot of Fig. 8 is, that at $T = 300$ K, the profile of G_M responses (solid symbols) are not identical for linear and saturation

TABLE 6. Bias and temperature dependent RMS error values between the modeled and the experimental transconductance of a 1 μm gate length SiC MESFET. Bold faces represent lowest error values.

Temp.	Model	V_{DS} 5 V	10 V	25 V	35 V	Avg.
$T = 300$ K	**Ahmed**	0.2532	**0.1241**	0.1786	0.3350	0.2519
	Proposed	**0.0850**	0.1271	**0.0188**	**0.0987**	**0.0824**
$T = 500$ K	**Ahmed**	**0.0649**	0.1270	0.0570	0.0898	0.0846
	Proposed	0.0685	**0.0872**	**0.0223**	**0.0521**	**0.0575**

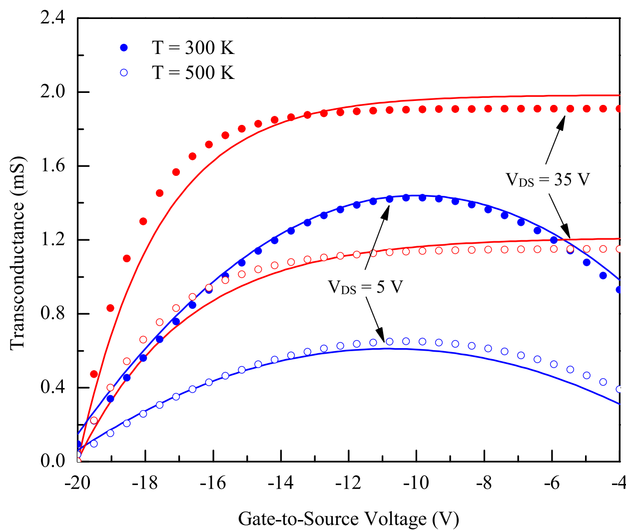

FIGURE 8. Measured (symbols) and modeled (lines) temperature dependent transconductance of a 1 μm gate length SiC MESFET.

region of operations. In the saturation region, the G_M profile gives a plateau for certain V_{GS} and then it approaches to zero, indicating that available channel crossection for the flow of carriers is diminishing with increasing magnitude of V_{GS}. On the other hand, in the linear region, where the carriers velocity is less than υ_s, the observed peak indicates that for such bias, $V_{GS} \approx -10$ V, the channel performs relatively better than other V_{GS} values.

Table 6 shows RMS error values, once again, for the two models under discussion. It is obvious from the average data of the table, that the proposed model offers a $\sim$ 67% improvement at $T = 300$ K and this value is $\sim$ 32% at $T = 500$. This data clearly show that the proposed model exhibits a significant improvement in predicting G_{MT} of a wide bandgap MESFET.

IV. CONCLUSION

An improved analytical model for wide bandgap power MESFETs is proposed to predict output and transfer characteristics. The proposed modified model incorporates negative conductance in the saturation region of operation caused by the device self-heating and harsh ambient environment where these devices are normally operated. It has been demonstrated that the proposed model can predict output characteristics even for submicron MESFETs with a good degree of accuracy. A comparative analysis showed that the developed technique offers $\sim$ 50% and $\sim$ 37% improvement in predicting the output characteristics of wide bandgap MESFETs at $T = 300$ K and $T = 500$ K, respectively, relative to the best reported model in the literature. Based on the developed $I-V$ expression, device output conductance and transconductance were also modeled. It has been shown that the proposed technique can model the device output conductance for the entire range of its operation, both at room as well as at elevated temperature with an improved accuracy. Thus, the proposed technique could be useful in assessing the temperature dependent characteristics of wide bandgap MESFETs, meant for high temperature operation.

REFERENCES

[1] J. Millán, P. Godignon, X. Perpiñà, and A. Pérez-Tomás, and J. Rebollo, "A survey of wide bandgap power semiconductor devices," *IEEE Trans. Power Electron.*, vol. 29, no. 5, pp. 2155–2163, May 2014.

[2] J. B. Casady and R. W. Johnson, "Status of silicon carbide (SiC) as a wide-bandgap semiconductor for high-temperature applications: A review," *Solid-State Electron.*, vol. 39, no. 10, pp. 1409–1422, Oct. 1996.

[3] N. Lakhdar and F. Djeffal, "New optimized dual-material (DM) gate design to improve the submicron GaN-MESFETs reliability in subthreshold regime," *Microelectron. Rel.*, vol. 52, no. 6, pp. 958–963, 2012.

[4] F. Djeffal and N. Lakhdar, "An improved analog electrical performance of submicron Dual-Material gate (DM) GaAs-MESFETs using multi-objective computation," *J. Comput. Electron.*, vol. 12, no. 1, pp. 29–35, Mar. 2013.

[5] A. S. Royet, T. Ouisse, B. Cabon, O. Noblanc, C. Arnodo, and C. Brylinski, "Self-heating effects in silicon carbide MESFETs," *IEEE Trans. Electron Devices*, vol. 47, no. 11, pp. 2221–2227, Nov. 2000.

[6] J. Kuzmík *et al.*, "Self-heating in GaN transistors designed for high-power operation," *IEEE Trans. Electron Devices*, vol. 61, no. 10, pp. 3429–3434, Oct. 2014.

[7] N. Sghaier, J.-M. Bluet, A. Souifi, G. Guillot, E. Morvan, and C. Brylinski, "Study of trapping phenomenon in 4H-SiC MESFETs: Dependence on substrate purity," *IEEE Trans. Electron Devices*, vol. 50, no. 2, pp. 297–302, Feb. 2003.

[8] S. Dutta, "A theoretical study on the temperature-dependent RF performance of a SiC MESFET," *Int. J. Electron.*, vol. 105, no. 7, pp. 1117–1128, Jul. 2018.

[9] P. G. Neudeck, R. S. Okojie, and L.-Y. Chen, "High-temperature electronics-a role for wide bandgap semiconductors?" *Proc. IEEE*, vol. 90, no. 6, pp. 1065–1076, Jun. 2002.

[10] S. Bose, A. Kumar, M. Gupta, and R. S. Gupta , "A complete analytical model of GaN MESFET for microwave frequency applications," *Microelectron. J.*, vol. 32, no. 12, pp. 983–990, Dec. 2001.
[11] S. P. Murray and K. P. Roenker, "An analytical model for SiC MESFETs," *Solid-State Electron.*, vol. 46, no. 10, pp. 1495–1505, Oct. 2002.
[12] C. L. Zhu, C. C. Tin, S. F. Yoon, and J. Ahn, "A three-region analytical model for short-channel sic mesfets," *Microelectron. Eng.*, vol. 83, no. 1, pp. 96–99, Jan. 2006.
[13] M. M. Ahmed, M. Riaz, and U. F. Ahmed, "An improved model for the **I–V** characteristics of submicron SiC MESFETs by evaluating the potential distribution inside the channel," *J. Comput. Electron.*, vol. 16, no. 3, pp. 514–525, Sep. 2017.
[14] D. A. Neamen, *Semiconductor Physics and Devices: Basic Principles*. New York, NY, USA: McGraw-Hill, 2012.
[15] H. Lv, Y. Zhang, Y. Zhang, and L.-A. Yang, "Analytic model of IV characteristics of 4H-SiC MESFETs based on multiparameter mobility model," *IEEE Trans. Electron Devices*, vol. 51, no. 7, pp. 1065–1068, Jul. 2004.
[16] M. Roschke and F. Schwierz, "Electron mobility models for 4H, 6H, and 3C SiC [MESFETs]," *IEEE Trans. Electron Devices*, vol. 48, no. 7, pp. 1442–1447, Jul. 2001.
[17] P. H. Ladbrooke and M. Design, *GaAs FETs and HEMTs*. Boston, MA, USA: Artech House, 1989, pp. 125–135.
[18] X. Cheng, M. Li, and Y. Wang, "An analytical model for current–voltage characteristics of AlGaN/GaN HEMTs in presence of self-heating effect," *Solid-State Electron.*, vol. 54, no. 1, pp. 42–47, Jan. 2010.
[19] C. Gaquiere, S. Trassaert, B. Boudart, and Y. Crosnier, "High-power GaN MESFET on sapphire substrate," *IEEE Microw. Guided Wave Lett.*, vol. 10, no. 1, pp. 19–20, Jan. 2000.

SAIF-UR REHMAN received the B.S. and M.S. degrees in electronic engineering from Mohammad Ali Jinnah University, Islamabad. He is currently pursuing the Ph.D. degree with the Capital University of Science and Technology (CUST), where he is currently involved in the modeling and simulation of high-frequency and high-power FETs.

He is also an Assistant Professor with Superior University, Lahore, where he is involved in research and teaching activities with the Department of Electrical Engineering. His research interests include microelectronics, microwave FETs modeling, and antenna design. He is a Registered Engineer with the Pakistan Engineering Council (PEC), Islamabad.

UMER F. AHMED received the B.S. degree (Hons.) in electrical engineering from the COMSATS Institute of Science and Technology, Islamabad, in 2017, and the M.S. degree in electrical engineering from the Capital University of Science and Technology (CUST), Islamabad, in 2019.

He is currently a Research Associate in microelectronics and RF engineering with the Department of Electrical Engineering, CUST, where he is also a Lecturer. His research interests include microelectronics, microwave FETs modeling, and antenna design. He is a Registered Engineer with the Pakistan Engineering Council (PEC), Islamabad.

MUHAMMAD M. AHMED received the Ph.D. degree in microelectronics from the University of Cambridge, U.K., in 1995.

He has supervised numerous M.S. and Ph.D. Research Projects. He joined academia as a Professor, the Chairman, the Dean, and the Executive Vice President. He is currently a Vice Chancellor with the Capital University of Science and Technology (CUST), Islamabad. His research interests include microelectronics, and microwave and RF engineering. He has authored more than 140 research papers in the fields of microelectronics and RF engineering.

Dr. Ahmed is a Fellow of the Institution of Engineering and Technology (IET), U.K., and a Chartered Engineer (CEng) from the U.K. Engineering Council. He holds the title of European Engineer (EUR.ING.) from the European Federation of the National Engineering Association (FEANI), Brussels. He is a Life Member of the PEC, Pakistan, and EDS and MTTS, USA.

MUHAMMAD N. KHAN received the B.S. degree in electrical engineering from the University of Engineering and Technology (UET) at Peshawar, the M.S. degree in electrical engineering from UET Taxila, Pakistan, and the Ph.D. degree in microelectronics from the Capital University of Science and Technology (CUST), Islamabad. He is currently an Assistant Professor with the Department of Electrical Engineering, UET Peshawar at Bannu Campus. He is also a Research Fellow with CUST. His research interests include high-frequency FETs and power devices.